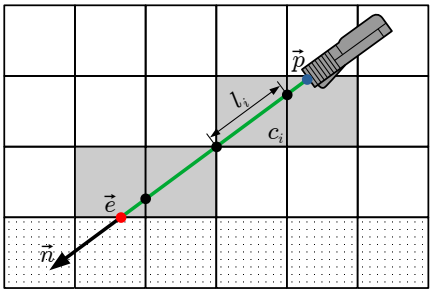

Fig. 2: Raytracing of a TDLAS beam through a 2D grid. The dotted cells represent obstacles, the grey cells are considered for the concentration estimation, the blue/red dot marks the start/end point of the ray and the black dots mark the intersection points of the ray with the gas concentration grid.

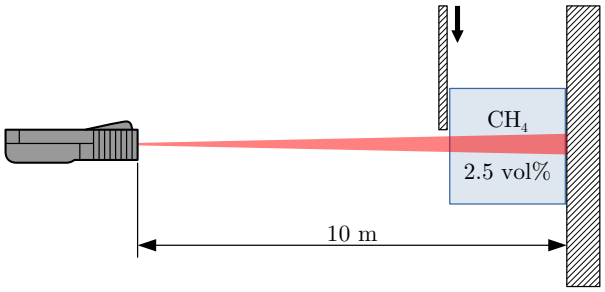

Fig. 3: Experiment setup. The obstacle between the remote gas sensor and the glass cube is moved in small steps until it fully hides the glass cube.

until it either hits an obstacle or the maximum measurement distance is reached. If an obstacle is hit, the ray becomes valid and its end point is given as $\vec{e} = \vec{p} + L \cdot \vec{n}$, where L is the length of the ray. During this process the gas concentration is integrated from $\vec{p}$ to $\vec{e}$ yielding the desired measurement value.

This simplified *Line Model*, however, does not account for the conical shape and the Gaussian intensity distribution of real laser beams. Therefore, we suggest to perform multiple line measurements in order to approximate the physical properties. A measurement by this *Cone Model* is given as

$$C = \frac{1}{\sum_i I_i} \sum_i \Bigg(I_i \underbrace{\sum_j c_{ij} l_{ij}}_{\text{Line Model}} \Bigg) + \varepsilon, \tag{1}$$

where c_{ij} is the concentration in the j-th traced cell of the i-th ray, l_{ij} is the length the beam traversed in that cell and ε is the sensor noise. The intensity of the i-th ray is given as

$$I_i = I_0 \frac{1}{L_i} \int_0^{L_i} \left(\frac{w_0}{w(z)} \right)^2 \exp\left(\frac{-2z^2 \sin^2(\vartheta_i)}{w(z)^2} \right) dz, \tag{2}$$

where L_i denotes the total length of ray i, w_0 and $w(z)$ are parameters of the beam, as shown in Fig. 1, and ϑ_i is the polar angle of the i-th ray with respect to the direction vector of the sensor, $\vec{n}$. For further details see [11].

III. Experiment Setup

To prove both the Gaussian intensity distribution of the laser beam and its conical shape, we set up the experiment shown in Fig. 3. A glass cube with edge length of 0.2 m is filled with a concentration of 2.5 vol% methane and is placed in front of a diffuse reflective wall. As remote gas sensor we use the LaserMethane mini-G (SA3C50A) from Tokyo Gas Engineering. According to its data sheet, the measuring laser has a wavelength of 1653 nm and a "beam extension" of 8.5 mrad or less. Since it is unclear whether this value denotes the divergence of the beam, θ, or the total angular spread of the beam, $\Theta = 2\theta$, we assume the larger value, i.e. $\Theta = 17\,\text{mrad}$.

The remote gas sensor is placed 10 m in front of the wall yielding a theoretical maximum spot size of 0.17 m. Due to its wavelength, the laser spot is not visible for humans. Therefore, we use a Goldeye short-wave infrared (SWIR) camera from Allied Vision with a spectral range from 900 nm to 1700 nm to centre the laser spot on the glass cube. In addition, we use the camera to take a video of the laser spot on the blank wall.

While the glass cube is fully exposed to the measuring laser at the beginning of the experiment, a diffuse reflective obstacle is moved in steps of 5 mm in front of the glass cube until the gas concentration is completely covered. For each step we take 400 measurements and calculate their mean value.

We expect the laser spot to have a Gaussian intensity distribution which is given in Cartesian coordinates as

$$g(x, y) = \frac{1}{\sqrt{4\pi^2\sigma^4}} \exp\left(-\frac{x^2 + y^2}{2\sigma^2} \right). \tag{3}$$

Let d denote the length of the overlap of the glass cube and the obstacle, such that there is no overlap for $d \leq 0\,\text{m}$ and the glass cube is fully masked for $d \geq 0.2\,\text{m}$. Then the portion of the total intensity that is not affected by the gas becomes

$$I_{\text{eff}} = \int_{-\infty}^{\infty} \int_{-\infty}^{d} g(x, y)\, \mathrm{d}x\, \mathrm{d}y \tag{4}$$

$$= \frac{1}{\sqrt{4\pi^2\sigma^4}} \int_{-\infty}^{\infty} \int_{-\infty}^{d} e^{-\frac{x^2}{2\sigma^2}} e^{-\frac{y^2}{2\sigma^2}}\, \mathrm{d}x\, \mathrm{d}y. \tag{5}$$

Since the second exponential function does not depend on d, we can solve the integral and incorporate it into a new coefficient K:

$$I_{\text{eff}} = K \int_{-\infty}^{d} \exp\left(-\frac{x^2}{2\sigma^2} \right) \mathrm{d}x. \tag{6}$$

This is similar to a shifted and scaled (Gauss) error function. We expect the gas concentration measurements taken with the TDLAS device during the experiment to match (6).

To compare the sensor model with the results of the real experiment, we create the same setup in the simulator. Although we investigated different ray configurations for the sensor model in [11], here we only consider the "reference" model with 131 rays, which is shown in Fig. 4a.

IV. Results

In Fig. 4b the average value of the 200 video frames taken of the laser spot are shown. In contrast to the expected diameter of 170 mm, the actual spot size is in the range of 60 mm, so the total angular spread is $\Theta \approx 6\,\mathrm{mrad}$ and thus within the range specified by the manufacturer. This result is also supported by the experiment with the moving obstacle. As soon as the obstacle had an influence on the gas measurements, increasing d by approximately 60 mm was sufficient to fully hide the gas concentration in the glass cube from the TDLAS sensor.

In Fig. 5 the intensity distribution summed over one axis and a Gaussian fitted to it are shown. The amplitude is normalised to 1 and the x-axis to the range [-1, 1]. Although there are some outliers, both curves are well correlated. These outliers are probably caused by the speckle pattern of the spot [12].

Fig. 6 shows the result of the experiment and the simulation as well as the integral of the curve obtained from the camera (Fig. 5). Since the camera measurement, experiment and simulation have different input scales, the data is fitted to a reference error function:

$$I_{\mathrm{eff,ref}} = \frac{1}{2}\left(\mathrm{erf}(5(d-1/2))+1\right). \tag{7}$$

Due to the shifting, the range [-∞, 0[has no significant contribution and is therefore neglected, such that (6) can be expressed with the standard error function, erf. Basically, all results match (7) with root mean square errors in the range of 10^{-3} to 10^{-2}, as shown in Tab. I.

Looking at the result of the simulator, one can observe conspicuous steps in the intensity plot yielding rather high errors. These are caused by the regular pattern of the ray configuration. Especially at the centre, where the Gaussian distribution has its highest intensity, significant jumps in the signal can be observed (Fig. 6, around $d = 0.5$). Moreover, the error of the simulation does not converge to 0. This is due to the fact that the background concentration is not modelled, which was in the range of 1% of the measured values during the experiments.

V. Conclusion

Both the experiment and the camera images prove the conical shape and Gaussian intensity distribution of the measuring laser of the remote gas sensor, which are the key assumptions of the novel TDLAS model.

The simulated experiment has shown that the sensor model has an average error in the range of 1%, which is perfectly sufficient for the use cases in the field of mobile robot olfaction. However, future work might include the evaluation of different ray configurations to further improve the model.

TABLE I: Root mean squared errors

	Camera	Simulation	Experiment
RMSE	$2.73 \cdot 10^{-3}$	$9.76 \cdot 10^{-3}$	$4.63 \cdot 10^{-3}$

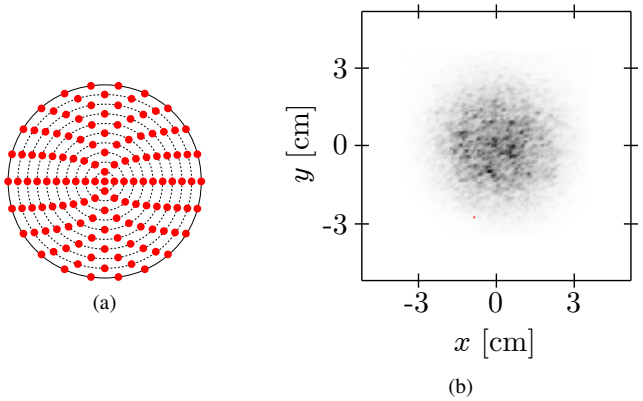

(a) (b)

Fig. 4: (a) Cross section of the sensor model beam. The red dots mark the positions of the single measurement rays within the cone. (b) Spot of the measuring laser on a blank wall.

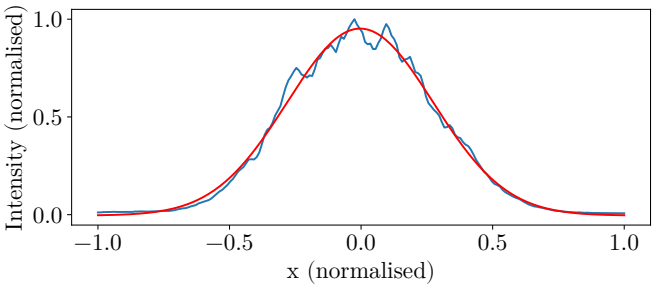

Fig. 5: Blue curve: The intensity distribution of the laser spot shown in Fig. 4b summed along its y-axis and normalised. Red curve: A fitted Gaussian.

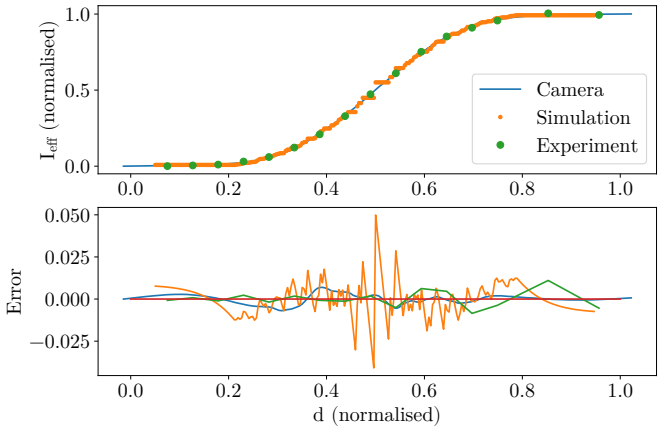

Fig. 6: Upper plot: Received intensity of the TDLAS sensor that is not affected by the gas depending on the position of the obstacle d. Lower plot: Errors of the curves in the upper plot with respect to the reference (Gauss) error function (7).

REFERENCES

[1] C. Sui, "Taiwan gas blasts in Kaohsiung kill at least 25," BBC News, 1 August, 2014. [Online]. Available: https://www.bbc.com/news/world-asia-28594693 [Accessed 18 June, 2019].

[2] H. Ishida, Y. Wada and H. Matsukura, "Chemical Sensing in Robotic Applications: A Review," IEEE Sensors Journal, vol. 12(11), pp. 3163–3173, November 2012.

[3] P. P. Neumann, H. Kohlhoff, D. Hüllmann, A. J. Lilienthal and M. Kluge, "Bringing Mobile Robot Olfaction to the Next Dimension - UAV-based Remote Sensing of Gas Clouds and Source Localization," Proceedings of the 2017 IEEE International Conference on Robotics and Automation (ICRA), pp. 3910–3916, 2017.

[4] P. P. Neumann, D. Hüllmann, D. Krentel, M. Kluge, H. Kohlhoff and A. J. Lilienthal, "Gas Tomography Up In The Air!," Proceedings of the IEEE Sensors 2018, pp. 396–398, 2018.

[5] V. H. Bennetts, E. Schaffernicht, T. Stoyanov, A. J. Lilienthal and M. Trincavelli, "Robot assisted gas tomography - Localizing methane leaks in outdoor environments," Proceedings of the 2014 IEEE International Conference on Robotics and Automation (ICRA), pp. 6362–6367, 2014.

[6] P. P. Neumann, H. Kohlhoff, D. Hüllmann, D. Krentel, M. Kluge, M. Dzierliński, A. J. Lilienthal and M. Bartholmai, "Aerial-based Gas Tomography - From Single Beams to Complex Gas Distributions," European Journal of Remote Sensing, 2019, to appear.

[7] M. A. Arain, E. Schaffernicht, V. H. Bennetts and A. J. Lilienthal, "The right direction to smell: Efficient sensor planning strategies for robot assisted gas tomography," Proceedings of the 2016 IEEE International Conference on Robotics and Automation (ICRA), pp. 4275–4281, 2016.

[8] M. A. Arain, H. Fan, V. H. Bennetts, E. Schaffernicht and A. J. Lilienthal, "Improving gas tomography with mobile robots: An evaluation of sensing geometries in complex environments," Proceedings of the 2017 ISOCS/IEEE International Symposium on Olfaction and Electronic Nose (ISOEN), 2017.

[9] H. Fan, M. A. Arain, V. H. Bennetts, E. Schaffernicht and A. J. Lilienthal, "Improving gas dispersal simulation for mobile robot olfaction: Using robot-created occupancy maps and remote gas sensors in the simulation loop," Proceedings of the 2017 ISOCS/IEEE International Symposium on Olfaction and Electronic Nose (ISOEN), 2017.

[10] J. Monroy, V. Hernandez-Bennetts, H. Fan, A. J. Lilienthal and J. Gonzalez-Jimenez, "GADEN: A 3D Gas Dispersion Simulator for Mobile Robot Olfaction," Sensors, vol. 17, no. 7, p. 1479, 2017.

[11] D. Hüllmann, P. P. Neumann, J. Monroy and A. J. Lilienthal, "A Realistic Remote Gas Sensor Model for Three-Dimensional Olfaction Simulations," Proceedings of the 2019 IEEE International Symposium on Olfaction and Electronic Nose (ISOEN), pp. 7–9, 2019.

[12] J. C. Dainty, Laser Speckle and Related Phenomena, 2nd ed., Springer, 1984.